THE JOURNAL OF PHYSICAL CHEMISTRY B

pubs.acs.org/JPCB Article

Cu(I) Controls Conformational States in Human Atox1 Metallochaperone: An EPR and Multiscale Simulation Study

Ortal Perkal,[‖] Zena Qasem,[‖] Meital Turgeman, Renana Schwartz, Lada Gevorkyan-Airapetov, Matic Pavlin, Alessandra Magistrato, Dan Thomas Major,* and Sharon Ruthstein*

Cite This: J. Phys. Chem. B 2020, 124, 4399−4411 Read Online

ACCESS | Metrics & More | Article Recommendations | Supporting Information

ABSTRACT: Atox1 is a human copper metallochaperone that is responsible for transferring copper ions from the main human copper transporter, hCtr1, to ATP7A/B in the Golgi apparatus. Atox1 interacts with the Ctr1 C-terminal domain as a dimer, although it transfers the copper ions to ATP7A/B in a monomeric form. The copper binding site in the Atox1 dimer involves Cys12 and Cys15, while Lys60 was also suggested to play a role in the copper binding. We recently showed that Atox1 can adopt various conformational states, depending on the interacting protein. In the current study, we apply EPR experiments together with hybrid quantum mechanics−molecular mechanics molecular dynamics simulations using a recently developed semiempirical density functional theory approach, to better understand the effect of Atox1's conformational states on copper coordination. We propose that the flexibility of Atox1 occurs owing to protonation of one or more of the cysteine residues, and that Cys15 is an important residue for Atox1 dimerization, while Cys12 is a critical residue for Cu(I) binding. We also show that Lys60 electrostatically stabilizes the Cu(I)−Atox1 dimer.

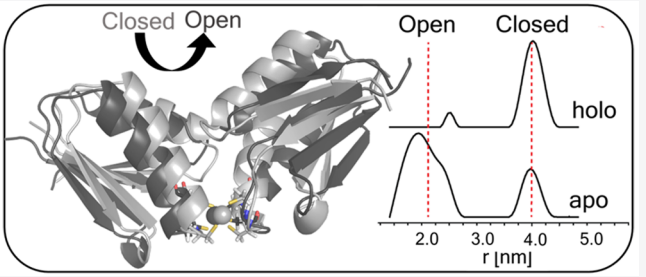

INTRODUCTION

Copper, like other metals, has a pivotal role in fundamental processes of cell function. It takes part in cellular respiration, iron oxidation, pigment formation, neurotransmitter biosynthesis, antioxidant defense, and connective tissue formation.[1,2] Yet, when present at excessive concentrations, it can endanger the cell's survival, by causing deregulated oxidation of proteins, lipids, and other cellular components, ultimately leading to injury. Moreover, free Cu ions can produce radical oxygen species (ROS), which can lead to cytotoxic interactions with cell membranes.[3−6] Thus, intracellular pathways of copper metabolism have evolved to ensure the appropriate amount of Cu for cell survival.[1,7]

In general, copper in the human body follows the following trajectory: First, it accumulates in the blood through diet. Once it has been inserted, it is taken up from the blood by the copper transporter hCtr1.[8,9] The copper is then reduced from its oxidized form, Cu(II), to the Cu(I) form.[10,11] Then, the transporter transfers the Cu(I) into the cell. Next, specific Cu(I) chaperones deliver the metal to the appropriate cellular pathways.[2,12−14] Atox1 is one of the chaperones responsible for delivering Cu(I) ions to ATP7A and ATP7B in the trans-Golgi network.[15] Atox1, also called Hah1, is a soluble protein (68 amino acids), displaying a $\beta\alpha\beta\beta\alpha\beta$ fold, and it coordinates one Cu(I) ion with the cysteine residues of a conserved 12Cxx15C motif.

Cu(I) uptake by Atox1 occurs via the C-terminal domain of hCtr1 which involves the 188HCH motif. NMR experiments revealed that Cu(I) binds to 188HCH with high affinity (K_D of 10^{-14} M).[16] As a result, Cu(I) can be released to its target by protein−protein interaction, while being unable to freely dissociate from hCtr1. Cu(I)'s binding affinity toward Atox1 is even higher than that for the C-terminal domain of hCtr1 ($K_D = 10^{-17.4}$ M), enabling Cu(I) to be transferred from hCtr1 to the metallochaperone.[17] Previously, we conducted electron paramagnetic resonance (EPR) measurements to resolve the various conformational states of Atox1,[18−20] showing that Atox1 is highly sensitive to its environment and target proteins and can accommodate distinct conformations (i.e., an open and a closed one).

EPR spectroscopy has emerged as an excellent tool for gaining structural information on proteins, since it does not require crystallization and does not depend on protein size. EPR's strength lies in its sensitivity to both atomic level changes and nanoscale fluctuations. EPR can characterize properties such as redox state and ligand geometry for different

Received: February 28, 2020
Revised: May 6, 2020
Published: May 12, 2020

https://dx.doi.org/10.1021/acs.jpcb.0c01744
J. Phys. Chem. B 2020, 124, 4399−4411

Table 1. Primers Used for Atox1 Mutants

mutation	forward primer	reverse primer
C12A	ATG CCG AAG CAC GAG TTC TCT GTG GAC ATG ACC GCT GGA GGC TGT GCT GAA GCT GTC TCT CGG GTC CTC AAT AAG	CTT ATT GAG GAC CCG AGA GAC AGC TTC AGC ACA GCC TCC AGC GGT CAT GTC CAC AGA GAA CTC GTG CTT CGG CAT
C15A	ATG CCG AAG CAC GAG TTC TCT GTG GAC ATG ACC TGT GGA GGC GCT GCT GAA GCT GTC TCT CGG GTC CTC AAT AAG	CTT ATT GAG GAC CCG AGA GAC AGC TTC AGC AGC GCC TCC ACA GGT CAT GTC CAC AGA GAA CTC GTG CTT CGG CAT
C12M	5-AAG CAC GAG TTC TCT GTG GAC ATG ACC ATG GGA GGC TGT GCT GAA GCT GTC TCT CGG-3	5-CCG AGA GAC AGC TTC AGC ACA GCC TCC CAT GGT CAT GTC CAC AGA GAA CTC GTG CTT-3
C15M	5-GAG TTC TCT GTG GAC ATG ACC TGT GGA GGC ATG GCT GAA GCT GTC TCT CGG GTC CTC AAT-3	5-ATT GAG GAC CCG AGA GAC AGC TTC AGC CAT GCC TCC ACA GGT CAT GTC CAC AGA GAA CTC-3
K60A	5-G AAA ACA GGA GCG ACT GTT TCC TAC CTT GGC CTT GAG-3	5-CTC AAG GCC AAG GTA GGA AAC AGT CGC TCC TGT TTT C-3

functional states of the protein and can measure distances between paramagnetic probes within the protein, and between proteins, up to 10 nm. The most common experiment for obtaining nanoscale structure information is the pulsed electron double resonance (PELDOR), also commonly referred to as the double electron−electron resonance experiment (DEER). Pulsed EPR experiments can measure nanometer distances between paramagnetic probes, and continuous wave (CW) EPR can derive the dynamics of protein chains. The combination of CW and pulsed EPR with site-directed spin-labeling (SDSL) has become widely used in biophysical research,[21−25] where an electron spin introduced into diamagnetic proteins provides information on their local environment and on the mobility of the protein domain. When multiple spin-labels are attached, distance distributions between them can be derived.[23−30]

Earlier works have addressed questions relating to copper binding in proteins using theoretical tools,[31−34] and in particular, the binding mode of Cu(I) to Atox1 has been studied theoretically by several researchers.[34−40] Reported coordination numbers vary between two and three, depending on the methods employed, as well as the state of the protein (monomer or dimer). Dalosto suggested that that Cu(I) is coordinated by 2 Cys residues in a near-linear arrangement, based on quantum mechanics−molecular mechanics (QM/MM) calculations on the Atox1 monomer.[37] Holt and Merz explored the coordination of Cu(I) in a small model system, containing methylthiolate (CH_3S-) and methylthiol (CH_3SH). These authors concluded on the basis of QM and classical molecular dynamics (MD) simulations that two- or three-coordination is preferred and four-coordination is unlikely in copper exchange.[39] Their calculations were performed in both vacuum and aqueous solution but did not take into account the effect of the protein environment. Shurki and co-workers[35] developed a quantitative method to predict copper coordination number in small thiolato complexes,[36] using ligands resembling the Cys residues found in Atox1.[41] Their calculations on Atox1 as a model protein showed that the most favorable state is two-coordinated. However, in this case, they relied on an Atox1 monomeric NMR structure, and in order to simulate the three-coordinated state they added an external "cysteine-like" ligand.

Recently, Ruthstein and co-workers published a combined experimental and computational study of copper trafficking in eukaryotic systems.[38,40] On the basis of classical MD simulations, they explored the transfer of copper to ATP7A/B in monomeric and heterodimeric states. Density functional theory (DFT)-based QM/MM MD simulations were also done to characterize the coordination state of Cu(I) in the Atox1/MDB3/4 adducts, to better understand the Cu(I) transfer mechanism, and this work agrees well with other studies.[15,42−44] In addition, it was found that key and conserved residues, such as Lys60, Thr11, and Met10, stabilize the structure of Atox1,[15,42−44] and that during the Cu(I) transfer between Atox1 and the metal binding domain of monomeric ATP7B, a tricoordinated intermediate, mediated by Lys60, is formed.[40,45−47] However, to date no studies modeling the coordination of Cu(I) in homodimeric Atox1 have been attempted. The Atox1 dimeric state was detected by X-ray crystallography,[15,48] and this dimer-state was found to be biologically active, and to interact with a partner protein in the human cell.[19,20] In this crystal structure, the coordination state is four. Herein, we conduct EPR experiments at various pH values and explore the effect of mutagenesis in the Cu(I) binding site on the Atox1 structure. These experiments are complemented by hybrid QM/MM MD simulations using a recently developed semiempirical DFT approach for copper,[49−54] to get a better understanding and perspective of copper binding forms in Atox1. This study provides additional information on the copper transfer mechanism through the Ctr1−Atox1−ATP7A/B cycle.

EXPERIMENTAL METHODS

Atox1 Cloning, Expression, Purification, and Labeling. The human Atox1 was expressed and purified as described before.[19,20,55] The construct pYTB12-Atox1 with an intein and a chitin binding domain was used. It was transformed to the *Escherichia coli* strain BL21 (DE3). The expression was performed in BL21 cells, which were grown to an optical density of 0.5−0.8 at 600 nm and were induced with 0.5 mM isopropyl-β-D-thiogalactopyranoside (Calbiochem) for 18 h at 18 °C. The cells were then harvested by centrifugation and suspended in lysis buffer (25 mM Na_2HPO_4, 150 mM NaCl, 20 μM PMSF pH 8.8). The cells were sonicated by 6 cycles of 1 min each, with a 1 min cooling tense between each cycle (65% amplitude). After sonication, cells were centrifuged, and the soluble fraction of the lysate was run through a chitin bead column (New England Biolabs), allowing the Atox1 fusion to bind to the resin via its chitin binding domain. 30-column volumes of lysis buffer (pH 8.8) were used to wash the resin. To induce the intein-mediated cleavage, the beads were incubated in 50 mM DTT, 25 mM Na_2HPO_4, pH 8.8, 150 mM NaCl, for 40 h at room temperature. Atox1 was then collected in elution fractions and analyzed by SDS PAGE (Tricine 14%). Before labeling, 10 mM DTT was added to the protein solution and mixed for 10 h at 4 °C. DTT was dialyzed out using 3 kDa dialysis cassettes (Pierce). *S*-(2,2,5,5-Tetramethyl-2,5-dihydro-^1H-pyrrol-3-yl)methyl methanesulfonothioate (MTSSL, TRC) was added to the protein solution (with 100-fold molar excess of MTSSL) in the presence of

https://dx.doi.org/10.1021/acs.jpcb.0c01744
J. Phys. Chem. B 2020, 124, 4399−4411

Cu(I), to prevent spin-labeling at Cys12 and Cys15 positions.[20] The protein solution was then vortexed overnight at 4 °C. The free spin-label was removed by several dialysis cycles over 4 days.

Atox1 Mutagenesis. Several point mutations were created: C12A, C15A, C12M, C15M, K60A. The amino acid switching was done by restriction free cloning using the primers described in Table 1.

The pH value was adjusted during the purification step by changing the pH of the lysis buffer.

CD. Circular dichroism (CD) measurements were performed using a Chirascan spectrometer (Applied Photophysics, UK) at room temperature. Measurements were carried out in a 1 cm optical path length cell. The data were recorded from 190 to 260 nm with a step size and a bandwidth of 1 nm. Spectra were obtained after background subtraction. CD measurements were conducted on Atox1 at different pH values (8, 8.8, 10).

Addition of the Metal Ion. Cu(I) (tetrakis(acetonitrile)-copper(I) hexafluorophosphate (Aldrich)) was added to a protein solution under nitrogen gas to preserve anaerobic conditions. The Cu(II) EPR signal was not observed at any time. At low-temperature measurements, 20% glycerol was added to the protein solution.

EPR. CW-EPR (continuous wave EPR) spectra were recorded using an E500 Elexsys Bruker X-band spectrometer operating at 9.0−9.5 GHz. The spectra were recorded at room temperature (295 ± 2 K) at a microwave power of 20.0 mW, a modulation amplitude of 1.0 G, a time constant of 60 ms, and a receiver gain of 60.0 dB. The samples were measured in 0.8 mm capillary quartz tubes (vitrocom). CW-EPR simulations were carried out with MATLAB, using the easyspin toolbox.[56]

The constant time four-pulse DEER experiment $\pi/2(\nu_{obs})-\tau_1-\pi(\nu_{obs})-t'-\pi(\nu_{pump})-(\tau_1+\tau_2-t')-\pi-(\nu_{obs})-\tau_2(\nu_{obs})-\tau_2-$echo was carried out at (50 ± 1.0 K) on a Q-band Elexsys E580 instrument (equipped with a 2 mm probehead). A two-step phase cycle was employed on the first pulse. The echo was measured as a function of t', while τ_2 was kept constant to eliminate relaxation effects. The observer pulse was set 60 MHz higher than the pump pulse. The observer $\pi/2$ and π pulses had a length of 40 ns, and the π pump pulse had a length of 40 ns as well, while the dwell time was 20 ns. The observer frequency was 33.81 GHz. The samples were measured in 1.6 mm capillary quartz tubes (Wilmad). The data were analyzed using the DeerAnalysis 2016 program, using Tikhonov regularization.[57]

Each monomer of Atox1 contains three cysteine residues. Cys12 and Cys15 are involved in the cysteine-bridge and cannot be labeled, whereas Cys41 is accessible for spin-labeling for EPR measurements. The most common spin-label to cysteine residues is methanesulfonothioate (MTSSL). All EPR data presented here were performed on a labeled Atox1 in Cys41 position with MTSSL.

COMPUTATIONAL METHODS

System Setup. The X-ray crystal structure of wild type (WT) Atox1 (PDB ID code: 1fee)[58] was used to construct the initial configuration for the present study. The setup and MD heating and equilibration simulations of all systems were carried out employing standard procedures.[59−61] Briefly, the protonation states of all polar amino acid residue side-chains were adjusted to pH ∼ 8.5, and the protonation states of the His residues (two neutral tautomeric forms) were determined on the basis of the hydrogen bonding patterns of the local environment. The pair of Cys12 and 15 residues was deprotonated, while the two Lys60 residues were protonated. The HBUILD facility in the program CHARMM was used to add hydrogen atoms.[62,63] The Atox1 protein was soaked in a solvent box of dimensions 65.0 × 65.0 × 65.0 Å^3. A total of 32 sodium ions and 29 chloride ions were added to the system to neutralize the overall negative charge, and this ionic concentration mimics experimental conditions and effectively screens the charges in the system.

Potential Energy Surface. The potential energy surface in the current study is described by a hybrid quantum mechanics−molecular mechanics (QM/MM) Hamiltonian,[64] where the QM region is treated by a modified SCC-DFTB semiempirical Hamiltonian[49−54] with recently developed parameters for copper. A QM/MM approach is key to being able to answer questions regarding the coordination state of copper in Atox1, as it treats the Cu−S interactions quantum mechanically, while also including all effects of the surrounding protein environment, water, and salt. The QM region includes the copper ion, and significant fragments of Atox1, which are proximal to the copper binding center (43 QM atoms, Figure 1), whereas the MM region contains the entire protein, water

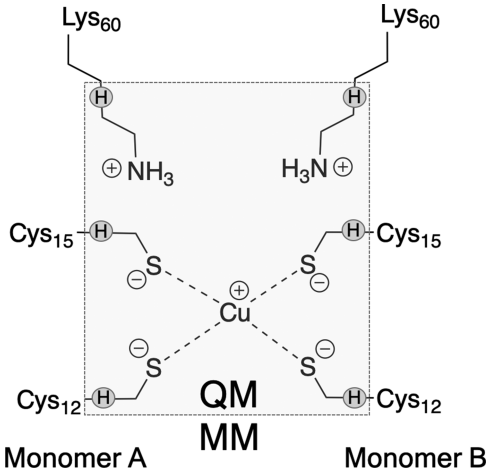

Figure 1. QM region (gray shade) contains 43 atoms from Cys12, Cys15, and Lys60 residues. The remaining system (protein, water, salt) is treated via MM.

molecules, and salt. The protein is treated using the CHARMM27 force field.[65−67] The water molecules were represented by the three-point charge TIP3P model.[68] In addition, six hydrogen link atoms were introduced along the covalent bonds crossing the boundary between the QM and the MM regions, to satisfy the valence requirements of the QM fragments. A schematic representation is depicted in Figure 1, where the quantum link atoms are circled. We note that chemical changes can only occur within the QM region, and hence, only proton transfer between QM atoms is possible. For instance, Cys protonation by bulk water cannot be observed with the current setup.

Simulation Protocols. Periodic boundary conditions were employed to solvate the Atox1−copper complex using a pre-equilibrated cubic water box, while long-range electrostatic interactions (both MM and QM/MM) were realized using the Ewald summation technique (64 × 64 × 64 FFT grid, κ = 0.340 Å^{-1}).[69] The system was fully minimized, heated up

https://dx.doi.org/10.1021/acs.jpcb.0c01744
J. Phys. Chem. B 2020, 124, 4399−4411

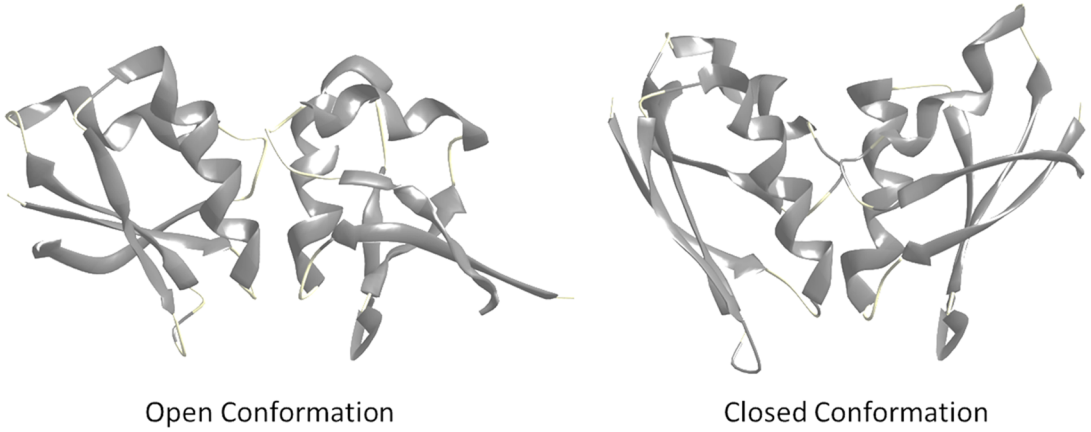

Figure 2. Two conformational states of Atox1 based on EPR data as reported in Levy et al.[19]

gradually to 298 K for 25 ps, and equilibrated for 3.5 ns at that temperature. During these simulations we applied four nuclear Overhauser effect (NOE) restraints on copper−sulfur (Cys12, 15) distances, in both protein monomers. The restraints were then removed, and an additional 16.5 ns MD was performed. This 20 ns trajectory was then used as a starting point for four additional independent MD simulations. The initial configurations were drawn from the 20 ns MD trajectory at time points 5, 10, 15, and 20 ns. In these additional four simulations, the velocities were randomized at the outset. All five simulations together provide ca. 100 ns of multiscale simulation time.

Heating simulations were performed in a canonical ensemble (NVT), whereas all subsequent simulations were conducted with the isothermal−isobaric (NPT) ensemble at 1 atm pressure and the target temperature was controlled by the extended constant pressure/temperature (CPT) method[70,71] and the Hoover thermostat.[72] The leapfrog integration scheme[73] was used to propagate the equations of motions, and the SHAKE algorithm[74] was applied to constrain all MM bonds involving hydrogen atoms, allowing a time step of 1 fs.

Umbrella Simulations. The umbrella sampling (US) technique[75] was used to determine the classical-mechanical potential of mean force (PMF), $\Delta G^{\ddagger}_{C}$, for the proton transfer between Lys60 and Cys15 of each of two monomers at 25 °C. In the current study, two different descriptions of the proton transfer were tested, one modeling a direct proton transfer between Lys60 and Cys15 and another via a bridging water molecule. In the latter case, the bridging water was included in the QM region. In all cases, the chemical reaction coordinate was defined as the antisymmetric reactive stretch coordinate, ζ_{asym}. The reaction coordinates were discretized and divided into 13 evenly spaced regions, or "windows", and each window was subject to an appropriate harmonic restraint, which keeps the reaction coordinate in the desired region. The chemical reaction coordinate bias was supplemented by an umbrella potential (roughly the negative of the PMF). To efficiently update the biasing potential as necessary, each window was sampled in multiple successive series with a predetermined number of MD steps. A typical simulation starts with a short equilibration (2 ps), followed by collection of the probability densities (ρ) of configurations along the reaction coordinates. Whenever the biasing potential was updated, the subsequent simulation commenced with a short 2 ps equilibration, and the accompanying equilibration data were discarded. The positions and velocities of the last recorded configuration in a specific window were used to start its successor, to maintain continuity of propagation. The cumulative simulation time per window was 500 ps, resulting in 7.5 ns sampling for each PMF profile. The statistics for the reaction coordinates were sorted into bins of width 0.01 Å. PMF profiles were computed using the weighted histogram analysis method (WHAM) (Figures S1 and S2, and Table S1).[60]

Trajectory Analysis. We obtained correlated motions in Atox1 by computing the atomic displacement covariance matrix. All the frames in each trajectory were reoriented to remove net translations and rotations during the simulations. Covariance matrices for the Cα atoms were calculated from all cumulative simulation data (100 ns of trajectory data). The covariance (C_{ij}) between two atoms i and j is given by eq 1:

$$C_{ij} = \langle (x_i - \langle x_i \rangle) \cdot (x_j - \langle x_j \rangle) \rangle \quad (1)$$

where x_i is the position of atom i. The normalized covariance (C_{ij}) is obtained by eq 2:

$$C_{ij} = C_{ij} / \sqrt{(C_{ii} C_{jj})} \quad (2)$$

We performed principal component analysis (PCA) on the simulation trajectory to filter out the fast, local fluctuations from the functionally relevant low-frequency collective motions of the protein using Bio3D combined with R.[76] This program calculates the principal components (orthogonal eigenvectors) that describe the axes of maximal variance from the distribution of superimposed structures. Further projection of the total distribution onto the selected eigenvector (subspace of largest principal component) results in a lower-dimensionality representation of the structural data set, allowing us to extract the functionally relevant motions from the trajectory. We extracted the principal motions from 100 ns QM/MM MD trajectories. The backbone C_α atoms were used for superposition of the Atox1 structures from the trajectory. The obtained collective motions were identified and are discussed in the Results section.

RESULTS

We have previously shown that Atox1 can exist in two conformation states:[19] One is a closed conformation, which is consistent with the crystal structure conformation,[77] and the second is an open conformation[19] (Figure 2). The open conformation is more flexible and can interact with various parts of the hCtr1 intracellular domains.[20,55] To better understand the interaction between Atox1 conformational

https://dx.doi.org/10.1021/acs.jpcb.0c01744
J. Phys. Chem. B 2020, 124, 4399−4411

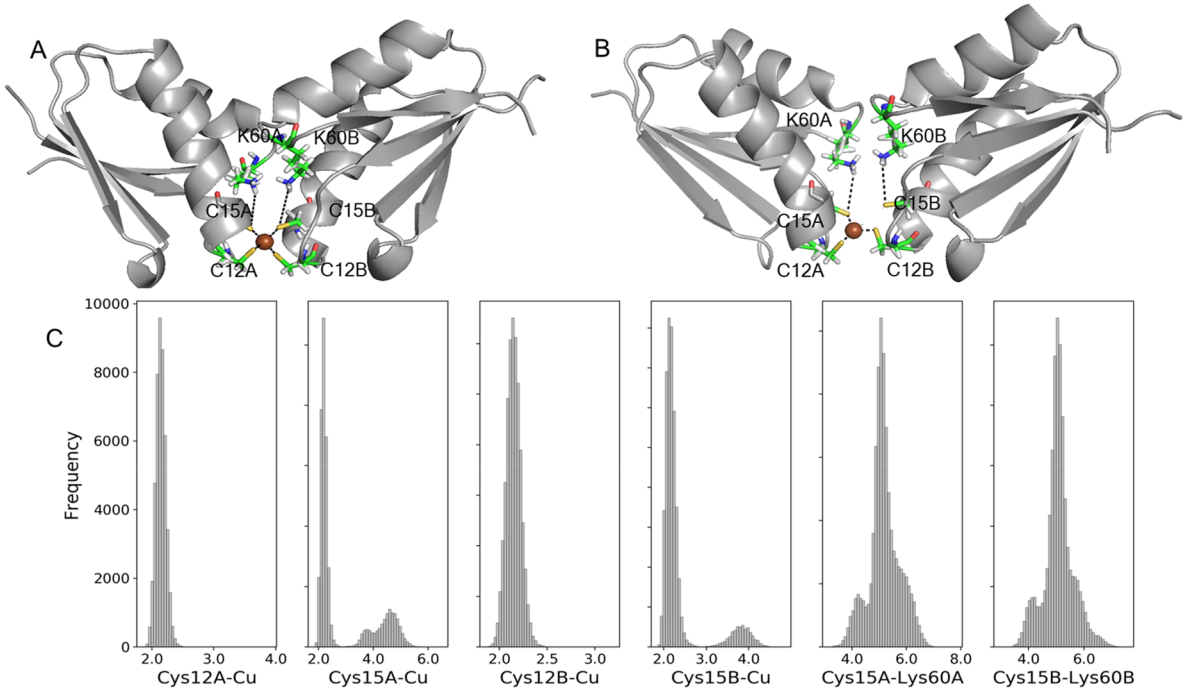

Figure 3. Illustration of coordination between Cu−Cys12,15 and Lys60−Cys15. (A) Four-coordination, (B) three-coordination, and (C) heavy-atom distance distributions from multiscale MD simulations.

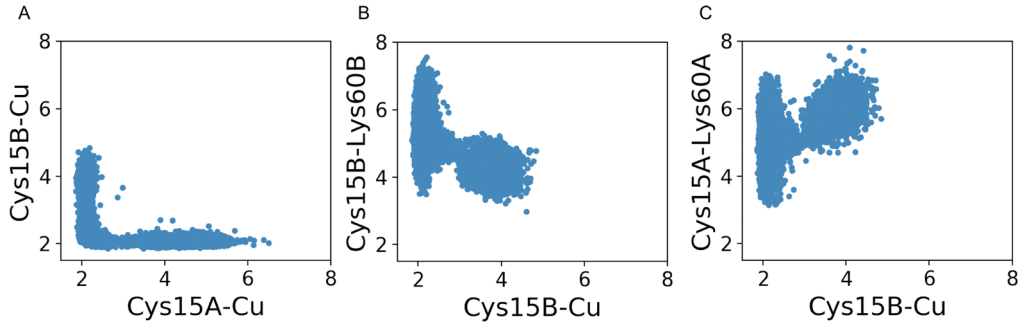

Figure 4. Distance (Å) correlation plots for Cys15 and Lys60 in Atox1.

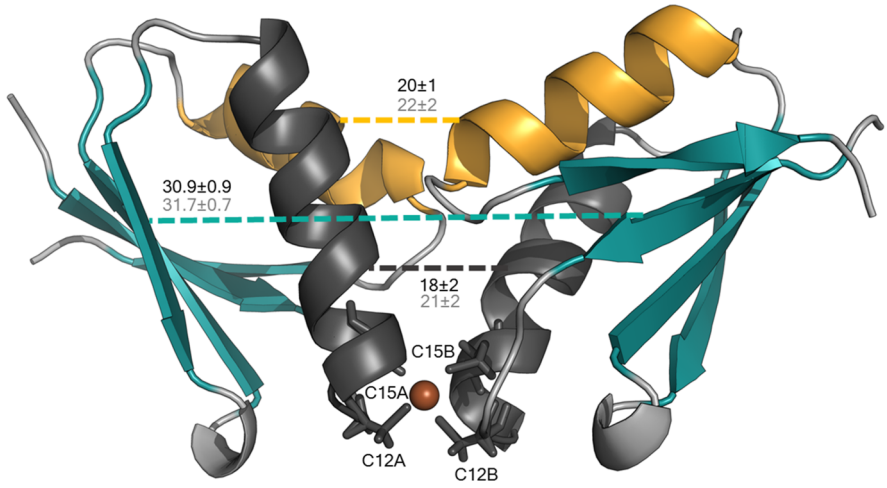

Figure 5. Ensemble averaged distances (Å) between the three main motifs in the two monomers in both coordination states (four-coordination, black; three-coordination, gray) of the Atox1 dimer.

states and copper coordination, we adopted a combined theoretical and experimental approach, as detailed below.

QM/MM MD Simulations of Atox1. The current multiscale (i.e., QM/MM) MD simulations commenced with

https://dx.doi.org/10.1021/acs.jpcb.0c01744
J. Phys. Chem. B 2020, 124, 4399−4411

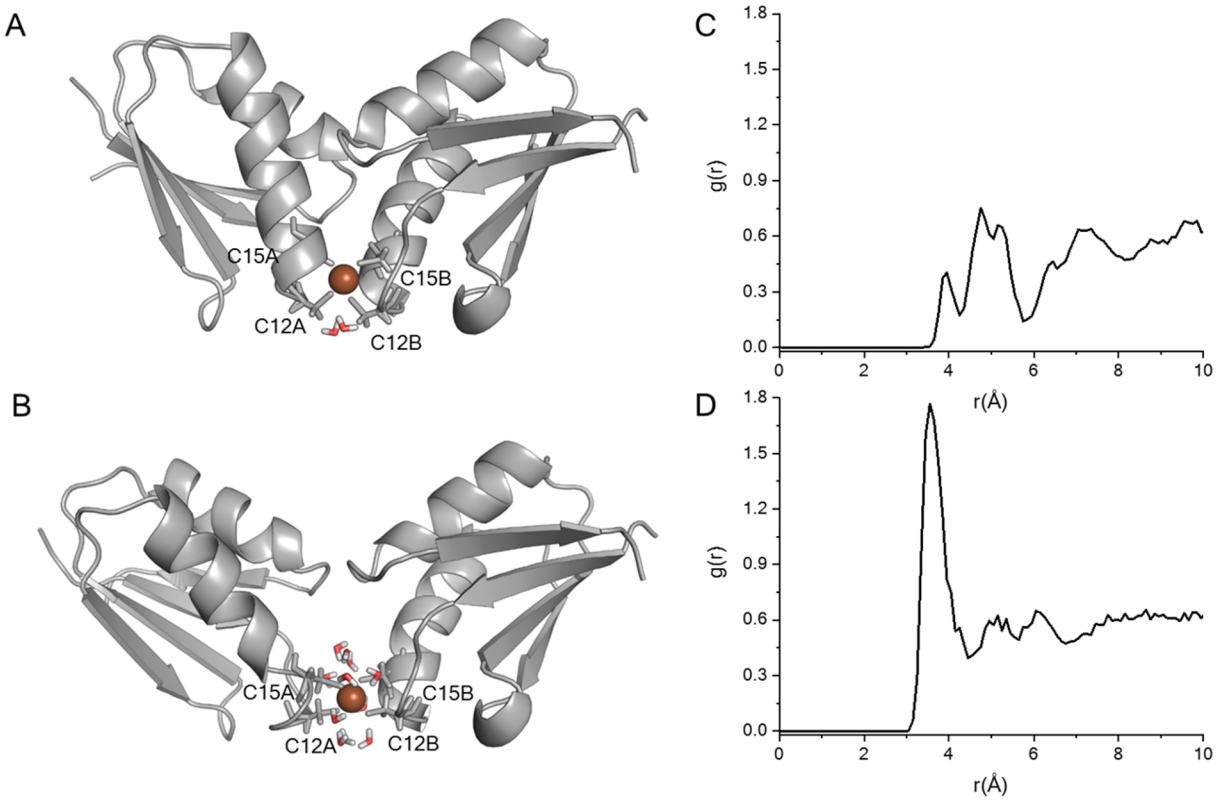

Figure 6. Water molecules in the copper binding site in Atox1. (A) Four-coordinated state, (B) three-coordinated state, (C) RDF for the four-coordinated state, (D) RDF for the three-coordinated state.

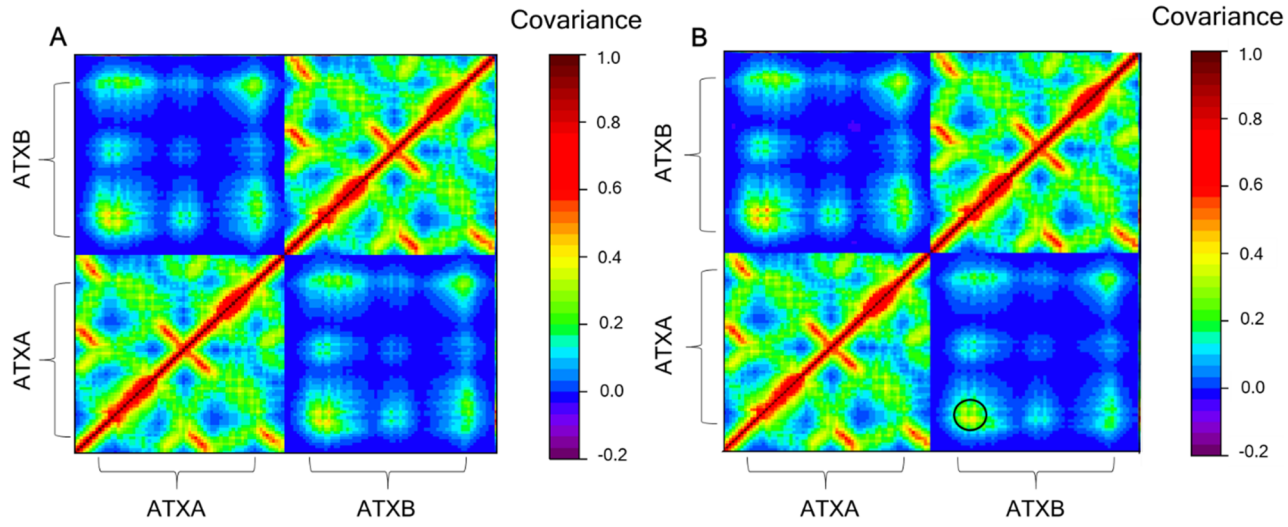

Figure 7. Covariance matrices for multiscale MD simulation data. (A) All data included. (B) Covariance matrix for the four-coordinated state (upper triangle) and for the three-coordinated state (lower triangle).

the four-coordinated crystal structure, which represents the closed state of Atox1. Due to the high cost of multiscale modeling and the consequent limited simulation time, the current simulations report mainly on the coordination of the closed state and the concomitant conformational changes of Atox1 in this state. A main finding of the current simulations is that Cu-coordination fluctuates between three- and four-coordinated states of Atox1 in the closed state (Figures S3−S7, and Tables S2 and S3). Figure 3 shows an illustration of both three- and four-coordination modes, as well as the distance probability distributions between copper and Cys12/15, and between Lys60 and Cys15 in each monomer. The Cu-Cys12 coordination is monomodal with average distances of 2.15 ± 0.01 Å. The Cu−Cys15 coordination is bimodal with average distances of 2.8 ± 0.1 Å. This bimodal distribution is a result of one of the two Cys15 residues flipping between the first and second shell coordination. The Lys60−Cys15 distance distribution is also bimodal, which is a result of the same flipping of Cys15 between first and second shell coordination. Key ensemble averaged distances are provided in Table S4.

To understand the correlation between the motion of Cys15 and Lys60, we plot the distribution of selected Cu−Cys15 and

https://dx.doi.org/10.1021/acs.jpcb.0c01744
J. Phys. Chem. B 2020, 124, 4399−4411

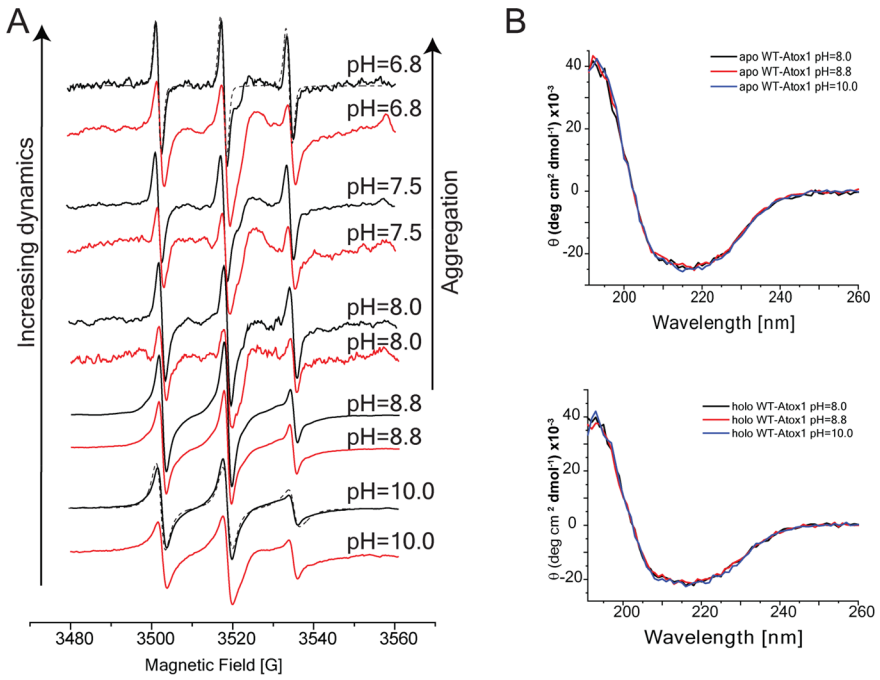

Figure 8. (A) RT X-band (9.79 GHz) CW-EPR spectra of Atox1 labeled at the Cys41 position with MTSSL in the absence of Cu(I) ion, the apo-state (black solid line), and in the presence of Cu(I), the holo-state (red solid line). The dashed lines for apo-Atox1 (pH = 10, and pH = 6.8) are simulated spectra using the parameters described in the text. (B) CD spectra of WT-Atox1 in the apo- and holo-states at various pH values.

Cys15−Lys60 distances (Figure 4). Several conclusions can be derived from this analysis: First, Cys15−Cu distances alternate between four-coordination and three-coordination, but no two-coordination is observed (Figure 4A). Second, weakening of the Cys15B−Cu interaction strengthens the Cys15B−Lys60B contact (Figure 4B) but at the same time weakens the Cys15A−Lys60A contact (Figure 4C). Hence, the relative motion of the moieties is correlated due to the tight interaction network between them, and Lys60 influences the effective pK_a of Cys15.

Next, we attempted to understand whether there is a connection between the coordination state of Cu in Atox1 and the ensemble averaged structure of the protein's secondary motifs (Figure 5). The three main motifs in the Atox1 dimer are two large α-helices, located at the center (dark gray), two smaller α-helices at the top (yellow), and two β-sheet strands (cyan). The distances in the four-coordinated state appear in black, while those for the three-coordination state are colored gray. All three interdomain distances are larger for the three-coordination state than for the four-coordinated state. This suggests that all motifs move slightly apart, indicating a breathing motion of the entire protein as a function of coordination state.

As a result of the monomer breathing motion as a function of coordination state, the copper binding site becomes increasingly accessible to water in the three-coordinated state. We analyze the hydration in the copper binding site by computing the radial distribution functions (RDFs) around the metal ion (Figure 6). The RDF reports on the water layers around the copper site and reveals that the binding site in the three-coordinated state is more accessible to water than in the four-coordinated state. The integrated value of the first peak of radial distribution function at a radius of ∼3.5 Å around copper is ca. 7 times greater for the three-coordinated state (Figure 6D) than for the four-coordinated state (Figure 6C). This further emphasizes the conformational change due to changes in copper coordination. This could allow protonation of Cys15 via water.

To further understand the motions in Atox1, we computed the cross-correlation matrix among all Cα atoms (Figure 7). The red color represents correlated motions where residues move in concert, whereas the blue color represents anticorrelated motions. In Figure 7A, we show the correlation map for all of our multiscale simulation data. As expected, the positive correlation is much more pronounced within each monomer than between monomers. Within monomers, we identify large regions that move in a correlated fashion (residues 38−45 and 60−68, both β strands, cyan color in Figure 5), but with less significant anticorrelated motion. Between monomers, we identify anticorrelated motion and also significant correlated motion between Cys12A−Cys12B, Cys12A−Cys15B, Cys15A−Cys12B, and Cys15A−Cys15B. Next, we divided the correlation maps into four- and three-coordinated triangular maps (Figure 7B). The upper triangle represents the four-coordinated case, while the lower triangle represents the three-coordinated case. Comparing the map of three-coordinated and four-coordinated copper, we see the disappearance of some red patches in the three-coordinated state (encircled in black). This indicates a partial loss of correlated motion in the three-coordinated state, which translates into a less ordered structure for this state. This difference in protein motion in the three- and four-coordinated states is also visible in the principal motions (Movie S1 and Movie S2).

Effect of pH on Cu(I) Binding and Atox1's Structure. In order to better understand the role of the various conformation states of Atox1 in Cu(I) transfer and binding, we conducted EPR experiments at various pH values, and we explored the effect of mutagenesis in the Cu(I) binding site on the Atox1 structure.

https://dx.doi.org/10.1021/acs.jpcb.0c01744
J. Phys. Chem. B 2020, 124, 4399−4411

The CW-EPR spectra of Atox1 (labeled at Cys41) at room temperature at various pH values, with (red line) and without (black line) the presence of Cu(I), are presented in Figure 8A. The CW-EPR spectra show a reduction in the dynamics of the spin-label with an increase in pH value. In addition, below pH of 8.8 the protein seems to be less stable. We detected a reduction in S/N values, specifically in the holo-case, where the protein is bound to a Cu(I) ion. This suggests that the protein aggregates at pH values lower than 8.8. CD spectra (Figure 8B), however, did not detect any changes in the secondary structure of the protein as a function of pH, suggesting that even if the protein is less stable in certain pH ranges, its secondary structure is still preserved. The Cu(I) binding site in Atox1 involves cysteine residues Cys12 and Cys15, with a pK_a value of 8.5. This indicates that when the cysteine residues are protonated, the protein is more dynamic and less stable. This could be suggestive of changes in the Cu(I) coordination state, binding site hydration, and Cys protonation, as suggested above from multiscale MD simulations. The EPR data could also be indicative of transformation from a dimeric to a monomeric state. We conducted simulations for the CW-EPR spectra for pH = 10 and pH = 6.8 in the apo-state, using slow-motion theory derived by Freed and co-workers[78] as implemented in the easyspin toolbox.[56] For all spectra, the **g**-tensor used was constant, **g** = [2.0087, 2.006, 2.0022]. The CW-EPR spectrum was simulated with one component for pH = 10 with a correlation time of 1×10^{-9} s, and an isotropic electron−electron interaction (ω_{ee}) of 5 MHz (corresponds to a distance of 2.2 nm), a_N = 16.5 G. At a pH = 6.8, the spectrum was simulated with two components, where 85% of the species are similar to pH = 10, while 15% have a smaller correlation time of 1×10^{-10} s and no dipolar coupling. The CW-EPR data suggest that, at low pH values, some of the Atox1 may not be in a dimeric state, and, in this state, the dynamics is higher. The interchange between monomeric and dimeric states at low pH values may cause instability and aggregation of the protein.

To further explore the conformational changes that Atox1 experiences as a function of pH, DEER experiments were carried out. The DEER distance distribution functions are presented in Figure 9. Since each Atox1 monomer is spin-labeled only at a single residue, Cys41, the presence of a dipolar interaction between spin-labels confirms that most of the Atox1 protein in solution is in the dimeric state; monomeric Atox1 might contribute to the background DEER signal, but not to the dipolar modulation. The DEER experiments at pH = 8.0 revealed a distance distribution of 2.0 ± 0.3 nm for the apo-state and 2.2 ± 0.3 nm for the holo-state. Increasing the pH value to 8.8 results in a bimodal distance distribution as reported before,[20] both for the apo- and the holo-states. One distribution is around 2.2 ± 0.3 nm, and the second is at 4.15 ± 0.2 nm. At pH = 10, for the apo-state we get a broad distribution at 2.2 ± 0.5 nm and a smaller narrow distribution at 4.15 ± 0.2 nm. In the holo-state at pH = 10, we observe a single distribution at 4.2 ± 0.2 nm. The DEER data propose that there are two dominating conformations: one corresponding to the distribution around 2.2 nm, and the second to the distribution around 4.15 nm. There are small changes in these distributions as a function of Cu(I) binding and pH values, which can report on Atox1 flexibility, but in general, Atox1 is fluctuating between these two conformations. Previously, we assigned the closed conformation of Atox1 to the 4.15 nm distribution, while the distribution around 2.2 nm was assigned to the open conformation.[19] We note that the

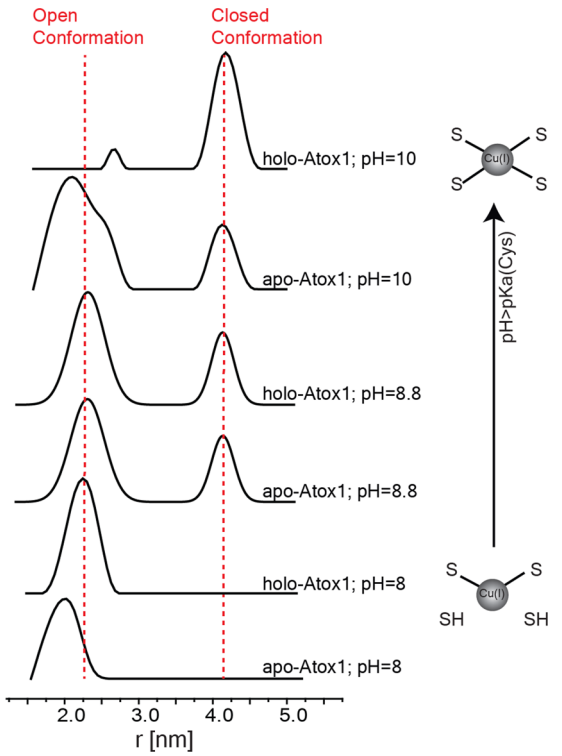

Figure 9. Q-band DEER distance distribution functions for apo- and holo-Atox1 at various pH values.

closed conformation is consistent with the crystal structure of Atox1. In human Atox1, the coordination of Cu(I) in the X-ray structure is a distorted tetrahedra with Cu···S distances of 2.3 Å for three of the cysteines, and 2.4 Å for the fourth cysteine. However, these distances are not distinguishable within the experimental uncertainty, and thus, Cu(I) can in principle be described as four-coordinated. This suggests that the flexibility of Atox1 occurs owing to protonation of one or more cysteine residues. These findings agree well with the above multiscale MD simulations, which suggest that Cu(I) exists in an equilibrium between the three- and four-coordinated states, and that the three-coordinated state has greater flexibility, as well as greater hydration of the copper binding site.

Role of Cys12 and Cys15 on Cu(I) Binding. In order to verify the importance of Cys12 and Cys15 residues to Cu(I) binding, we introduce C12A, C12M and C15A, C15M mutations. In order to prevent spin-labeling of Cys12 or Cys15 (when these residues are not mutated), the spin-labeling procedure was done in the presence of Cu(I) ion. After spin-labeling, various dialysis steps were performed to get rid of the bound Cu(I) ion. BCA UV−vis measurements confirmed the absence of Cu(I) ions after dialysis. CW-EPR spectra of the apo- and holo-forms of Atox1_C15A are characterized by an increase in dynamics compared to WT and the disappearance of the dipolar interaction (Figure 10). This suggests that, in the presence of C15A, Atox1 is in a monomeric state. Indeed, the DEER signal of apo-C15A did not show any dipolar modulation, demonstrating that Atox1 is in a monomeric state when the C15A mutation is present (data not shown). In addition, in the presence of Cu(I), a reduction in the S/N ratio was observed suggesting aggregation of the protein, and instability in the presence of C15A mutation and Cu(I). In the presence of C15M mutation, the protein is a bit more stable and also partially in a dimeric state in the presence of Cu(I)

https://dx.doi.org/10.1021/acs.jpcb.0c01744
J. Phys. Chem. B 2020, 124, 4399−4411

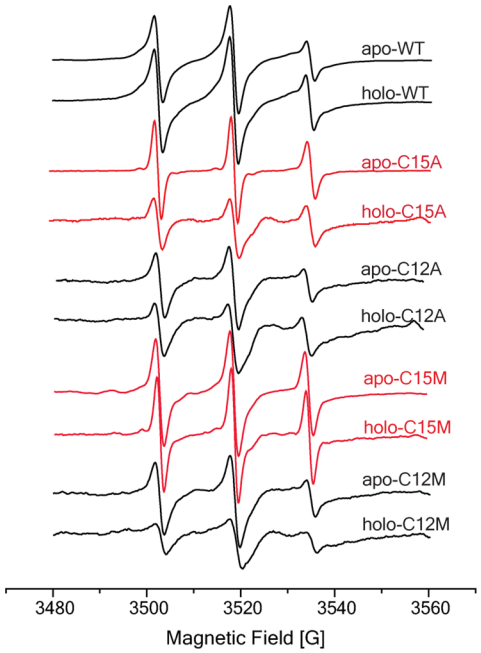

Figure 10. CW-EPR spectra of the apo- and holo-states of Atox1 in its WT and mutant forms.

ion (holo-state), suggesting that this mutation partially retrieves the functionality of Atox1. C12A and C12M mutations do not affect dimerization of Atox1; however, the instability of the protein greatly increased in the presence of Cu(I), and aggregation appears. In conclusion, the CW-EPR experiments suggest that the Cys15 residue is important for Atox1 dimerization, while Cys12 is important for the protein's stability in the presence of Cu(I), suggesting that Cys12 is critical for Cu(I) binding. This could be because Cys15 coordinates deeper inside the protein and is therefore an important anchor point for the dimer, whereas Cys12 is closer to the protein surface and therefore less critical for dimerization. Recently, Shoshan et al.[79] measured the dissociation constants of Cu(I) to Atox1 as a function of C12A and C15A mutations. They showed that C12A mutation dramatically decreased the affinity of copper to Atox1 by 2−3 orders of magnitude, while the C15A mutation only mildly affected copper affinity, and these findings agree nicely with the current EPR data. In addition, these data also agree with the QM/MM MD simulations, which found that Cys12 coordination is present at all times, while Cys15 fluctuates between coordinated and free states (Figures 3 and 4).

Role of Lys60 on Cu(I) Binding. A previous NMR solution structure study indicated that the K60A mutation causes crucial structural perturbations in the arrangement of secondary structures and the orientation of side-chains, including the metal binding sites formed by Cys12 and Cys15.[43] Protein dynamics studies revealed that the K60A mutation results in a change in protein flexibility mainly at residues around the metal binding site.[80,81] NMR titrations indicated that although both WT-Atox1 and the K60A mutant can deliver cuprous ion to the target protein MBD4 (the fourth metal binding domain in ATP7A/B), a different dynamic process could occur during the copper transfer.[82,83] In order to check the effect of the K60 residue on the Atox1 dimerization and conformation, we performed EPR experiments on the mutant protein.

Figure 11A presents CW-EPR measurements carried out on K60A Atox1. The spectrum of apo Atox1_K60A is similar to

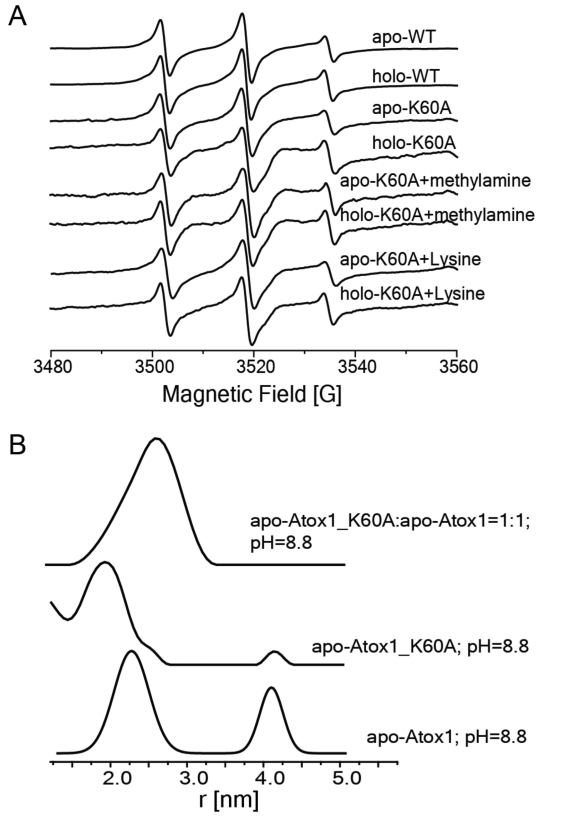

Figure 11. (A) RT CW-EPR spectra of WT-Atox1 and Atox1_K60A mutants labeled at the Cys41 position with MTSSL in the absence and presence of Cu(I) ion. (B) DEER distance distribution functions for WT-Atox1 and Atox1_K60A in the apo-form.

apo WT-Atox1, indicating no change in dynamics of Atox1 in the presence of this mutation. However, after adding Cu(I) to the Atox1_K60A mutation, part of the protein starts aggregating, suggesting that it is less stable with the K60A mutation. If we perform the "rescue test"[84] and add either methylamine or free Lys amino acid to the solution, we observe that in the presence of methylamine a lower S/N appeared both in the apo- and holo-states, suggesting that the protein is less stable in the presence of this single amine group. However, in the presence of lysine (which contains two amine groups), we observe a higher S/N suggesting less Atox1 aggregation in the holo-form, i.e., partial rescue of the Lys60 function. Figure 11B shows the DEER distance distribution of apo-Atox1_K60A. The population of the closed conformation (around 4.15 nm) is much smaller and almost negligible compared to WT-Atox1, suggesting that Lys60 is important for electrostatic stabilization of the four-sulfur coordination of Cu(I). In addition, we detected a shift in the open conformation to a lower distance distribution function. When mixing between WT-Atox1 and Atox1_K60A at a ratio of 1:1, a broad distribution between 2.0 and 3.0 nm appears, suggesting that the dimer is distorted. The multiscale simulations also support the role of Lys60 as stabilizing Cys15 via electrostatic interactions, as exemplified by the correlated motions between these residues (Figure 4).

We also tested the feasibility of a proton transfer between Lys60 and Cys15 within the same monomer. To this end, we

https://dx.doi.org/10.1021/acs.jpcb.0c01744
J. Phys. Chem. B 2020, 124, 4399−4411

performed QM/MM PMF simulations, gradually biasing the proton transfer process to occur during the limited simulation time. On the basis of the obtained PMF, we conclude that such a process is not likely as the barrier for proton transfer is too high, and the Cys15-Lys60 ion pair is preferred over the neutral pair (SI, Figure S1). This agrees with the experimental results, which showed that Lys60 is important for Atox1 dimer stabilization; however, Atox1 can still bind Cu(I) in the presence of the K60A mutation.

DISCUSSION

To maintain homeostasis, the human cell relies on ion binding metallochaperones to move Cu(I) as a complexed metal. The proteins that bind Cu(I) are highly specific, and most have a conserved CXXC motif. One such metallochaperone is Atox1, which is responsible for moving Cu(I) ions from the uptake copper transporter, hCtr1, to the six metal binding domains (MBDs) in the N-terminal region of ATP7A/B in the Golgi apparatus. We previously showed that Atox1 can accommodate various conformational states depending on its interacting protein.[19,20,55] We also showed that Atox1 interacts as a dimer with the Ctr1 C-terminal domain (intracellular part), but as a monomer with MBDs of ATP7B.[40] The ability of Atox1 to flip between two conformations on the basis of its target protein is important for preserving the tight in-cell copper concentration. Herein, we aimed to further resolve the copper binding site in the Atox1 dimer. Pulsed and CW-experiments showed that Atox1 preserves its dimerization even at a low pH value of 6.8. However, at pH values lower than 8.0, the protein is less stable and tends to aggregate, despite having an intact secondary structure. We also saw that the Cu(I) binding site cycles between two main configurations, one named the "closed conformation", which is prevalent at high pH values and agrees well with the X-ray structure.[77] Therefore, we can assign it as a four-coordinated sulfur-bound Cu(I) state. This was further supported by extensive QM/MM MD simulations. When lowering the pH value, the "open configuration" state becomes the dominant state. In this state, α2 and β4 are further apart from each other; Cu(I) is either three or two sulfur coordinated, and the structure is more flexible. Hints of this state were obtained from the QM/MM MD simulations, which identified a three-coordinated state, which has greater flexibility and copper binding site hydration than the four-coordinated state. The flexibility of the open state conformation was detected by a broader distance distribution function in the pulsed EPR data, and greater dynamics of the spin-labels by the CW-EPR data. This increased flexibility as a function of the Cu(I)-coordination state was also observed in our QM/MM MD simulations. Additionally, the simulations show that, in a partially open conformation, water molecules penetrate into the Cu(I) binding site area, which could possibly facilitate protonation of Cys15. Previously, we showed that when point mutations exist in the hCtr1 C-terminal domain, in order to still interact with hCtr1 and to induce metal transfer, Atox1 accommodates the "open conformation" state. This proposes that the "open state" conformation is highly important for preserving copper homeostasis, and for allowing copper transfer between hCtr1 and Atox1.

We then further investigated the effect of C12A/M and C15A/M mutations on Cu(I) binding and Atox1 dimerization. We showed that upon C15A/M mutation Atox1 is in a monomeric state, while C12A/M mutations identified Cys12 as a critical residue for Cu(I) binding, as was also detected by others.[79] Therefore, we believe that Cys15 is responsible for the fluctuation between the open and closed conformations.

As a conserved residue, Lys60 was suggested to play a role in stabilization of the negative charge distribution around the copper binding site. Badarau et al.[85] explored the affinity of Cu(I) for Atox1 in the pH 6−11 range, and the effect of K60A mutation on copper affinity. The experiments showed a first order increase in copper affinity to Atox1 with an increase in pH value from 6.1 to 9.0, followed by a plateau. This indicates that even protonation of a single cysteine residue affects the affinity of copper to Atox1. Moreover, the data showed that K60A also affects Cu(I) affinity to Atox1 and indicated that Lys60 is responsible for lowering the pK_a value of the cysteine residues in the CXXC motif of Atox1, allowing higher affinity of Cu(I) for Atox1. Lys60 was also suggested to play a role in stabilizing the charges when Cu(I) is bound and to assist in the copper transfer from Atox1 to MBDs in ATP7A/B.[40,80,81,86] Using EPR experiments, we explored the effect of K60A mutation on the open and closed conformations. We saw that, in the presence of this mutation, Atox1 is still a dimer, although the closed conformation disappeared. We also showed that Cu(I) can still bind to Atox1 in the presence of the K60A mutation; however, in this situation the protein is less electrostatically stable, and aggregation occurs. PMF simulations showed that proton exchange between Cys15 and Lys60 is less likely to occur, confirming that Atox1 can still bind Cu(I) in the presence of the K60A mutation.

Therefore, we conclude that both Cys15 and Lys60 play some role in the interchange between the closed and open states, or between the four-sulfur Cu(I) coordinated state to the three/two-sulfur coordinated states.

CONCLUSIONS

In summary, on the basis of experimental EPR and computational multiscale simulation results, we propose that Cu(I) binding in the closed Atox1 dimer flips between three- and four-coordinated sulfur−Cu(I) states, whereas in the open state Atox1 exists in an equilibrium of two- and three-coordinated states. The transformation between the open and closed states is likely triggered by thermal fluctuations of the protein as it flips between the four-, three-, and two-coordination states. Increasingly reduced copper coordination is accompanied by increased copper binding site hydration and subsequent Cys15 protonation, which favors the open state.

ASSOCIATED CONTENT

Supporting Information

The Supporting Information is available free of charge at https://pubs.acs.org/doi/10.1021/acs.jpcb.0c01744.

Figures and tables analyzing data from QM/MM simulations and additional experimental data (PDF)

Movie of Atox1 three-coordination principal movement (MP4)

Movie of Atox1 four-coordination principal movement (MP4)

AUTHOR INFORMATION

Corresponding Authors

Dan Thomas Major − *Department of Chemistry and Institute for Nanotechnology & Advanced Materials, Bar-Ilan University, Ramat-Gan 52900, Israel*; Phone: 972-3-5317684; Email: majort@biu.ac.il

https://dx.doi.org/10.1021/acs.jpcb.0c01744
J. Phys. Chem. B 2020, 124, 4399−4411

Sharon Ruthstein − *Department of Chemistry, Faculty of Exact Sciences, Bar Ilan University, Ramat-Gan 5290002, Israel;* orcid.org/0000-0002-1741-6892; Phone: 973-3-7384329; Email: Sharon.ruthstein@biu.ac.il

Authors

Ortal Perkal − *Department of Chemistry and Institute for Nanotechnology & Advanced Materials, Bar-Ilan University, Ramat-Gan 52900, Israel*

Zena Qasem − *Department of Chemistry, Faculty of Exact Sciences, Bar Ilan University, Ramat-Gan 5290002, Israel*

Meital Turgeman − *Department of Chemistry, Faculty of Exact Sciences, Bar Ilan University, Ramat-Gan 5290002, Israel*

Renana Schwartz − *Department of Chemistry and Institute for Nanotechnology & Advanced Materials, Bar-Ilan University, Ramat-Gan 52900, Israel*

Lada Gevorkyan-Airapetov − *Department of Chemistry, Faculty of Exact Sciences, Bar Ilan University, Ramat-Gan 5290002, Israel*

Matic Pavlin − *CNR-IOM at SISSA, 34135 Trieste, Italy*

Alessandra Magistrato − *CNR-IOM at SISSA, 34135 Trieste, Italy;* orcid.org/0000-0002-2003-1985

Complete contact information is available at: https://pubs.acs.org/10.1021/acs.jpcb.0c01744

Author Contributions

‖O.P. and Z.Q. contributed equally to the work.

Notes

The authors declare no competing financial interest.

■ ACKNOWLEDGMENTS

We acknowledge the support of ERC-STG, Grant 754365, given to S.R. We thank Prof. Q. Cui and Dr. D. Roston for help with use of SCCDFTB parameters for Cu(I). We thank Dr. Walke for help with UV−vis measurements.

■ REFERENCES

(1) Boal, A. K.; Rosenzweig, A. C. Structural Biology of Copper Trafficking. *Chem. Rev.* **2009**, *109*, 4760−4779.

(2) Burkhead, J. L.; Gogolin Reynolds, K. A.; Abdel-Ghany, S. E.; Cohu, C. M.; Pilon, M. Copper Homeostasis. *New Phytol.* **2009**, *182*, 799−816.

(3) Ahuja, A.; Dev, K.; Tanwar, R. S.; Selwal, K. K.; Tyagi, P. K. Copper mediated neurological disorder: visions into amyotrophic lateral sclerosis, Alzheimer and Menkes disease. *J. Trace Elem. Med. Biol.* **2015**, *29*, 11−23.

(4) Gaggelli, E.; Kozlowski, H.; Valensin, D.; Valensin, G. Copper homeostasis and neurodegenerative disorder (Alzheimer's, Prion, and Parkinson's Diseases and Amyotropic Lateral Sclerosis). *Chem. Rev.* **2006**, *106*, 1995−2044.

(5) Lutsenko, S. Human copper homeostasis: a network of interconnected pathways. *Curr. Opin. Chem. Biol.* **2010**, *14*, 211−217.

(6) Prohaska, J. R. Role of Copper Transporters in Copper Homeostasis. *Am. J. Clin. Nutr.* **2008**, *88*, 826S−829S.

(7) De Feo, C. J.; Aller, S. G.; Unger, V. M. A Structural Perspective on Copper Uptake in Eukaryotes. *BioMetals* **2007**, *20*, 705−716.

(8) Shenberger, Y.; Shimshi, A.; Ruthstein, S. EPR spectroscopy shows that the blood carrier protein, human serum albumin, closely interacts with the N-terminal domain of the copper transporter, Ctr1. *J. Phys. Chem. B* **2015**, *119*, 4824−4830.

(9) Stefaniak, E.; Plonka, D.; Drew, S. C.; Bossak-Ahmad, K.; Haas, K. L.; Pushie, M. J.; Faller, P.; Wezynfeld, N. E.; Bal, W. The N-terminal 14-mer model peptide of human Ctr1 can collect Cu(ii) from albumin. Implications for copper uptake by Ctr1. *Metallomics* **2018**, *10* (12), 1723−1727.

(10) Haas, K. L.; Putterman, A. B.; White, D. R.; Thiele, D. J.; Franz, K. J. Model Peptides Provide New Insights into the Role of Histidine Residues as Potential Ligands in Human Cellular Copper Acquisition via Ctr1. *J. Am. Chem. Soc.* **2011**, *133*, 4427−4437.

(11) Shenberger, Y.; Marciano, O.; Gottlieb, H.; Ruthstein, S. Insights into the N-terminal Cu(II) and Cu(I) binding sites of the human copper transporter CTR1. *J. Coord. Chem.* **2018**, *71*, 1985−2002.

(12) Puig, S.; Thiele, D. J. Molecular Mechanisms of Copper Uptake and Distribution. *Curr. Opin. Chem. Biol.* **2002**, *6*, 171−180.

(13) Robinson, N. J.; Winge, D. R. Copper Metallochaperones. *Annu. Rev. Biochem.* **2010**, *79*, 537−562.

(14) Rosenzweig, A. C. Copper Delivery by Metallochaperone Proteins. *Acc. Chem. Res.* **2001**, *34*, 119−128.

(15) Wernimont, A. K.; Huffman, D. L.; Lamb, A. L.; O'Halloran, T. V.; Rosenzweig, A. C. Structural basis for copper transfer by the metallochaperone for the Menkes/Wilson disease proteins. *Nat. Struct. Biol.* **2000**, *7* (9), 766.

(16) Kahra, D.; Kovermann, M.; Wittung-Stafshede, P. The C-terminus of human copper importer Ctr1 acts as a binding site and transferes copper to Atox1. *Biophys. J.* **2016**, *110*, 95−102.

(17) Brose, J.; La Fontaine, S.; Wedd, A. G.; Xiao, Z. Redox sulfur chemistry of the copper chaperone Atox1 is regulated by the enzyme glutaredoxin 1, the reduction potential of the glutathione couple GSSG/GSH and the availability of Cu(I). *Metallomics* **2014**, *6*, 793−808.

(18) Levy, A. R.; Nissim, M.; Mendelman, N.; Chill, J.; Ruthstein, S. Ctr1 intracellualr loop is involved in copper transfer mechanism to the Atox1 metallochaperone. *J. Phys. Chem. B* **2016**, *120*, 12334−12345.

(19) Levy, A. R.; Turgeman, M.; Gevorkyan-Aiapetov, L.; Ruthstein, S. The structural flexibility of the human copper chaperone Atox1: Insights from combined pulsed EPR studies and computations. *Protein Sci.* **2017**, *26*, 1609−1618.

(20) Levy, A. R.; Yarmiayev, V.; Moskovitz, Y.; Ruthstein, S. Probing the Structural Flexibility of the Human Copper Metallochaperone Atox1 Dimer and Its Interaction with the CTR1 C-Terminal Domain. *J. Phys. Chem. B* **2014**, *118*, 5832−5842.

(21) Cai, Q.; Kusnetzow, A. K.; Hubbell, W. L.; Haworth, I. S.; Gacho, G. P. C.; Van Eps, N.; Hideg, K.; Chambers, E. J.; Qin, P. Z. Site-directed spin labeling measurements of nanometer distances in nucleic acids using a sequence-independent nitroxide probe. *Nucleic Acids Res.* **2006**, *34* (17), 4722−4730.

(22) Columbus, L.; Hubbell, W. L. A new spin on protein dynamics. *Trends Biochem. Sci.* **2002**, *27* (6), 288−295.

(23) Mchaourab, H. S.; Oh, K. J.; Fang, C. J.; Hubbell, W. L. Conformation of T4 lysozyme in studied by site-directed spin labeling. *Biochemistry* **1997**, *36*, 307−316.

(24) Shin, Y.-K.; Levinthal, C.; Levinthal, F.; Hubbell, W. L. Colicin E1 binding to membranes: time-resolved studies of spin-labeled mutants. *Science* **1993**, *259*, 960−963.

(25) Vamvouka, M.; Cieslak, J.; Van Eps, N.; Hubbell, W.; Gross, A. The Structure of the Lipid-Embedded Potassium Channel Voltage Sensor Determined by Double-Electron-Electron Resonance Spectroscopy. *Protein Sci.* **2008**, *17* (3), 506−517.

(26) Altenbach, C.; Kusnetzow, A. K.; Ernst, O. P.; Hofmann, K. P.; Hubbell, W. L. High resolution distance mapping in rhodopsin reveals the pattern of helix movement due to activation. *Proc. Natl. Acad. Sci. U. S. A.* **2008**, *105*, 7439−7444.

(27) Cornish, V. W.; Benson, D. R.; Altenbach, C. A.; Hideg, K.; Hubbell, W. L.; Schultz, P. G. Site-specific incorportaion of biophysical probes into proteins. *Proc. Natl. Acad. Sci. U. S. A.* **1994**, *91*, 2910−2914.

(28) Stone, K. M.; Townsend, J. E.; Sarver, J.; Sapienza, P. J.; Saxena, S.; Jen-Jacobson, L. Electron spin resonance shows common structural features for different classes of EcoRI-DNA complexes. *Angew. Chem., Int. Ed.* **2008**, *47*, 10192−10194.

(29) Zou, P.; Bortolus, M.; Mchaourab, H. S. Conformational Cycle of the ABC Transporter MsbA in Liposoms: Detailed Analysis using

Double Electron Electron Resonance Spectroscopy. *J. Mol. Biol.* **2009**, *393*, 586−597.
(30) Pliotas, C.; Ward, R.; Branigan, E.; Rasmussen, A.; Hagelueken, G.; Huang, H.; Black, S. S.; Booth, I. R.; Schiemann, O.; Naismith, J. H. Conformational state of the MscS mechanosensitive channel in solution revealed by pulsed electron-electrin double resonance (PELDOR) spectroscopy. *Proc. Natl. Acad. Sci. U. S. A.* **2012**, *109*, E2675−E2682.
(31) Sousa, S. F.; Pinto, G. R.; Ribeiro, A. J.; Coimbra, J. T.; Fernandes, P. A.; Ramos, M. J. Comparative analysis of the performance of commonly available density functionals in the determination of geometrical parameters for copper complexes. *J. Comput. Chem.* **2013**, *34* (24), 2079−2090.
(32) Click, T. H.; Ponomarev, S. Y.; Kaminski, G. A. Importance of electrostatic polarizability in calculating cysteine acidity constants and copper (I) binding energy of Bacillus subtilis CopZ. *J. Comput. Chem.* **2012**, *33* (11), 1142−1151.
(33) Álvarez-Barcia, S.; Kästner, J. Copper coordination in formylglycine generating enzymes. *Eur. Phys. J.: Spec. Top.* **2019**, *227* (14), 1657−1664.
(34) Pitts, A. L.; Hall, M. B. Investigating the electronic structure of the Atox1 copper (I) transfer mechanism with density functional theory. *Inorg. Chem.* **2013**, *52* (18), 10387−10393.
(35) Ansbacher, T.; Shurki, A. Predicting the coordination number within copper chaperones: Atox1 as case study. *J. Phys. Chem. B* **2012**, *116* (15), 4425−4432.
(36) Ansbacher, T.; Srivastava, H. K.; Martin, J. M.; Shurki, A. Can DFT methods correctly and efficiently predict the coordination number of copper (I) complexes? A case study. *J. Comput. Chem.* **2010**, *31* (1), 75−83.
(37) Dalosto, S. D. Computer Simulation of the Interaction of Cu (I) with Cys Residues at the Binding Site of the Yeast Metallochaperone Cu (I)− Atx1. *J. Phys. Chem. B* **2007**, *111* (11), 2932−2940.
(38) Magistrato, A.; Pavlin, M.; Qasem, Z.; Ruthstein, S. Copper trafficking in eukaryotic systems: Current knowledge from experimental and computational efforts. *Curr. Opin. Struct. Biol.* **2019**, *58*, 26−33.
(39) Op't Hol, B. T.; Merz, K. M. Insights into Cu (I) exchange in HAH1 using quantum mechanical and molecular simulations. *Biochemistry* **2007**, *46* (30), 8816−8826.
(40) Qasem, Z.; Pavlin, M.; Ritacco, I.; Gevorkyan-Airapetov, L.; Magistrato, A.; Ruthstein, S. The pivotal role of MBD4-ATP7B in the human Cu(I) excretion path as revealed by EPR experiments and all-atom simulations. *Metallomics* **2019**, *11*, 1288−1297.
(41) Kohner-Kerten, A.; Tshuva, E. Y. Preparation and X-ray characterization of two-coordinate Cu (I) complex of aliphatic thiolato ligand: Effect of steric bulk on coordination features. *J. Organomet. Chem.* **2008**, *693* (11), 2065−2068.
(42) Rodriguez-Granillo, A.; Wittung-Stafshede, P. Differential roles of Met10, Thr11, and Lys60 in structural dynamics of human copper chaperone Atox1. *Biochemistry* **2009**, *48* (5), 960−972.
(43) Xi, Z.; Shi, C.; Tian, C.; Liu, Y. Conserved residue modulates copper-binding properties through structural dynamics in human copper chaperone Atox1. *Metallomics* **2013**, *5* (11), 1566−1573.
(44) Palm-Espling, M. E.; Niemiec, M. S.; Wittung-Stafshede, P. Role of metal in folding and stability of copper proteins in vitro. *Biochim. Biophys. Acta, Mol. Cell Res.* **2012**, *1823* (9), 1594−1603.
(45) Rodriguez-Granillo, A.; Crespo, A.; Estrin, D. A.; Wittung-Stafshede, P. Copper-transfer mechanism from the human chaperone Atox1 to a metal-binding domain of Wilson disease protein. *J. Phys. Chem. B* **2010**, *114* (10), 3698−3706.
(46) Banci, L.; Bertini, I.; Cantini, F.; Della-Malva, N.; Migliardi, M.; Rosato, A. The different intermolecular interactions of the soluble copper-binding domains of the Menkes protein, ATP7A. *J. Biol. Chem.* **2007**, *282* (32), 23140−23146.
(47) Strausak, D.; Howie, M. K.; Firth, S. D.; Schlicksupp, A.; Pipkorn, R.; Multhaup, G.; Mercer, J. F. Kinetic analysis of the interaction of the copper chaperone Atox1 with the metal binding sites of the Menkes protein. *J. Biol. Chem.* **2003**, *278* (23), 20821−20827.
(48) Anastassopoulou, I.; Banci, L.; Bertini, I.; Cantini, F.; Katsari, E.; Rosato, A. Solution structure of the apo and copper (I)-loaded human metallochaperone HAH1. *Biochemistry* **2004**, *43* (41), 13046−13053.
(49) Cui, Q.; Elstner, M.; Kaxiras, E.; Frauenheim, T.; Karplus, M. A QM/MM implementation of the self-consistent charge density functional tight binding (SCC-DFTB) method. *J. Phys. Chem. B* **2001**, *105* (2), 569−585.
(50) Yang, Y.; Yu, H.; York, D.; Cui, Q.; Elstner, M. Extension of the self-consistent-charge density-functional tight-binding method: third-order expansion of the density functional theory total energy and introduction of a modified effective coulomb interaction. *J. Phys. Chem. A* **2007**, *111* (42), 10861−10873.
(51) Gaus, M.; Cui, Q.; Elstner, M. DFTB3: extension of the self-consistent-charge density-functional tight-binding method (SCC-DFTB). *J. Chem. Theory Comput.* **2011**, *7* (4), 931−948.
(52) Gaus, M.; Cui, Q.; Elstner, M. Density functional tight binding: application to organic and biological molecules. *Wiley Interdiscip. Rev. Comp. Mol. Sci.* **2014**, *4* (1), 49−61.
(53) Gaus, M.; Jin, H.; Demapan, D.; Christensen, A. S.; Goyal, P.; Elstner, M.; Cui, Q. DFTB3 parametrization for copper: The importance of orbital angular momentum dependence of Hubbard parameters. *J. Chem. Theory Comput.* **2015**, *11* (9), 4205−4219.
(54) Jin, H.; Goyal, P.; Das, A. K.; Gaus, M.; Meuwly, M.; Cui, Q. Copper Oxidation/Reduction in Water and Protein: Studies with DFTB3/MM and VALBOND Molecular Dynamics Simulations. *J. Phys. Chem. B* **2016**, *120* (8), 1894−1910.
(55) Levy, A. R.; Nissim, M.; Mendelman, N.; Chill, J.; Ruthstein, S. Ctr1 Intracellular Loop Is Involved in the Copper Transfer Mechanism to the Atox1 Metallochaperone. *J. Phys. Chem. B* **2016**, *120* (48), 12334−12345.
(56) Stoll, S.; Schweiger, A. EasySpin, a Comprehensive Software Package for Spectral Simulation and Analysis in EPR. *J. Magn. Reson.* **2006**, *178* (1), 42−55.
(57) Jeschke, G. *Deeranalysis 2006: Distance Measurements on Nanoscopic Length Scales by Pulse ESR*; Springer, 2007; Vol. *27*, pp 287−288.
(58) Boal, A. K.; Rosenzweig, A. C. Crystal structure of cisplatin bound to human copper chaperone. *J. Am. Chem. Soc.* **2009**, *131*, 14196−14197.
(59) Doron, D.; Major, D. T.; Kohen, A.; Thiel, W.; Wu, X. Hybrid quantum and classical simulations of the dihydrofolate reductase catalyzed hydride transfer reaction on an accurate semi-empirical potential energy surface. *J. Chem. Theory Comput.* **2011**, *7* (10), 3420−3437.
(60) Doron, D.; Kohen, A.; Major, D. T. Collective reaction coordinate for hybrid quantum and molecular mechanics simulations: a case study of the hydride transfer in dihydrofolate reductase. *J. Chem. Theory Comput.* **2012**, *8* (7), 2484−2496.
(61) Doron, D.; Stojkovic, V.; Gakhar, L.; Vardi-Kilshtain, A.; Kohen, A.; Major, D. T. Free energy simulations of active-site mutants of dihydrofolate reductase. *J. Phys. Chem. B* **2015**, *119* (3), 906−916.
(62) Brooks, B. R.; Bruccoleri, R. E.; Olafson, B. D.; States, D. J.; Swaminathan, S. a.; Karplus, M. CHARMM: a program for macromolecular energy, minimization, and dynamics calculations. *J. Comput. Chem.* **1983**, *4* (2), 187−217.
(63) Brooks, B. R.; Brooks, C. L., III; Mackerell, A. D., Jr; Nilsson, L.; Petrella, R. J.; Roux, B.; Won, Y.; Archontis, G.; Bartels, C.; Boresch, S. CHARMM: the biomolecular simulation program. *J. Comput. Chem.* **2009**, *30* (10), 1545−1614.
(64) Warshel, A.; Levitt, M. Theoretical studies of enzymic reactions: dielectric, electrostatic and steric stabilization of the carbonium ion in the reaction of lysozyme. *J. Mol. Biol.* **1976**, *103* (2), 227−249.
(65) Best, R. B.; Zhu, X.; Shim, J.; Lopes, P. E.; Mittal, J.; Feig, M.; MacKerell, A. D., Jr Optimization of the additive CHARMM all-atom protein force field targeting improved sampling of the backbone ϕ, ψ

https://dx.doi.org/10.1021/acs.jpcb.0c01744
J. Phys. Chem. B 2020, 124, 4399−4411

and side-chain χ1 and χ2 dihedral angles. *J. Chem. Theory Comput.* **2012**, *8* (9), 3257−3273.
(66) MacKerell, A. D., Jr Empirical force fields for biological macromolecules: overview and issues. *J. Comput. Chem.* **2004**, *25* (13), 1584−1604.
(67) MacKerell, A. D., Jr; Bashford, D.; Bellott, M.; Dunbrack, R. L., Jr; Evanseck, J. D.; Field, M. J.; Fischer, S.; Gao, J.; Guo, H.; Ha, S. All-atom empirical potential for molecular modeling and dynamics studies of proteins. *J. Phys. Chem. B* **1998**, *102* (18), 3586−3616.
(68) Jorgensen, W. L.; Chandrasekhar, J.; Madura, J. D.; Impey, R. W.; Klein, M. L. Comparison of simple potential functions for simulating liquid water. *J. Chem. Phys.* **1983**, *79* (2), 926−935.
(69) Nam, K.; Gao, J.; York, D. M. An efficient linear-scaling Ewald method for long-range electrostatic interactions in combined QM/MM calculations. *J. Chem. Theory Comput.* **2005**, *1* (1), 2−13.
(70) Andersen, H. C. Molecular dynamics simulations at constant pressure and/or temperature. *J. Chem. Phys.* **1980**, *72* (4), 2384−2393.
(71) Feller, S. E.; Zhang, Y.; Pastor, R. W.; Brooks, B. R. Constant pressure molecular dynamics simulation: the Langevin piston method. *J. Chem. Phys.* **1995**, *103* (11), 4613−4621.
(72) Hoover, W. G. Canonical dynamics: Equilibrium phase-space distributions. *Phys. Rev. A: At., Mol., Opt. Phys.* **1985**, *31* (3), 1695.
(73) Hockney, R. W. The potential calculation and some applications. *Methods Comput. Phys.* **1970**, *9*, 136.
(74) Ryckaert, J.-P.; Ciccotti, G.; Berendsen, H. J. Numerical integration of the cartesian equations of motion of a system with constraints: molecular dynamics of n-alkanes. *J. Comput. Phys.* **1977**, *23* (3), 327−341.
(75) Torrie, G. M.; Valleau, J. P. Nonphysical sampling distributions in Monte Carlo free-energy estimation: Umbrella sampling. *J. Comput. Phys.* **1977**, *23* (2), 187−199.
(76) Grant, B. J.; Rodrigues, A. P.; ElSawy, K. M.; McCammon, J. A.; Caves, L. S. Bio3d: an R package for the comparative analysis of protein structures. *Bioinformatics* **2006**, *22* (21), 2695−2696.
(77) Boal, A. K.; Rosenzweig, A. C. Crystal structures of cisplatin bound to human copper chaperone. *J. Am. Chem. Soc.* **2009**, *131*, 14196−14197.
(78) Schnider, D. J.; Freed, J. H. In *Biological Magnetic Resonance. Spin Labeling*; Plenum: New York, 1989; Vol. *8*, Chapter 1.
(79) Shoshan, M. S.; Dekel, N.; Goch, W.; Shalev, D. E.; Danieli, T.; Lebendiker, M.; Bal, W.; Tshuva, E. Y. Unbound position II in MXCXXC metallochaperone model peptides impacts metal binding mode and reactivity: Distinct similarities to whole proteins. *J. Inorg. Biochem.* **2016**, *159*, 29−36.
(80) Rodriguez-Granillo, A.; Wittung-Stafshede, P. Structure and dynamics of Cu(I) binding in copper chaperones Atox1 and CopZ: a computer simulation study. *J. Phys. Chem. B* **2008**, *112* (15), 4583−93.
(81) Rodriguez-Granillo, A.; Wittung-Stafshede, P. Differential roles of Met10, Thr11, and Lys60 in structural dynamics of human copper chaperone Atox1. *Biochemistry* **2009**, *48* (5), 960−72.
(82) Rodriguez-Granillo, A.; Crespo, A.; Estrin, D. A.; Wittung-Stafshede, P. Copper-Transfer Mechanism from the Human Chaperone Atox1 to a Metal-Binding Domain of Wilson Disease Protein. *J. Phys. Chem. B* **2010**, *114*, 3698−3706.
(83) Arumugam, K.; Crouzy, S. Dynamics and Stability of the Metal Binding domains of the Menkes ATPase and their interaction with metallochaperone HAH1. *Biochemistry* **2012**, *51*, 8885−8906.
(84) Toney, M. D.; Kirsch, J. F. Direct Brønsted analysis of the restoration of activity to a mutant enzyme by exogenous amines. *Science* **1989**, *243*, 1485−1488.
(85) Badarau, A.; Dennison, C. Copper Trafficking mechanism of CXXC-containing domains: insight from the pH-dependence of their Cu(I) affinities. *J. Am. Chem. Soc.* **2011**, *133*, 2983−2988.
(86) Pavlin, M.; Qasem, Z.; Sameach, H.; Gevorkyan-Airapetov, L.; Ritacco, I.; Ruthstein, S.; Magistrato, A. Unraveling the Impact of Cysteine-to-Serine Mutations on the Structural and Functional Properties of Cu(I)-Binding Proteins. *Int. J. Mol. Sci.* **2019**, *20* (14), 3462.

https://dx.doi.org/10.1021/acs.jpcb.0c01744
J. Phys. Chem. B 2020, 124, 4399−4411